HAL
open science

Two case studies of winter continental-type water and mixed-phase stratocumuli over the sea 1. Microphysical and optical properties

Jean-François Gayet, Shoji Asano, Akihiro Yamazaki, Akihiro Uchiyama, Alexander Sinyuk, Olivier Jourdan, Frédérique Auriol

To cite this version:

Jean-François Gayet, Shoji Asano, Akihiro Yamazaki, Akihiro Uchiyama, Alexander Sinyuk, et al.. Two case studies of winter continental-type water and mixed-phase stratocumuli over the sea 1. Microphysical and optical properties. Journal of Geophysical Research: Atmospheres, 2002, 107 (D21), pp.AAC 11-1 - AAC 11-15. 10.1029/2001JD001106 . hal-01825027

HAL Id: hal-01825027

https://hal.science/hal-01825027v1

Submitted on 11 Jan 2021

HAL is a multi-disciplinary open access archive for the deposit and dissemination of scientific research documents, whether they are published or not. The documents may come from teaching and research institutions in France or abroad, or from public or private research centers.

L'archive ouverte pluridisciplinaire **HAL**, est destinée au dépôt et à la diffusion de documents scientifiques de niveau recherche, publiés ou non, émanant des établissements d'enseignement et de recherche français ou étrangers, des laboratoires publics ou privés.

Two case studies of winter continental-type water and mixed-phase stratocumuli over the sea 1. Microphysical and optical properties

Jean-François Gayet,[1] Shoji Asano,[2] Akihiro Yamazaki,[3] Akihiro Uchiyama,[3] Alexander Sinyuk,[4] Olivier Jourdan,[1] and Frédérique Auriol[1]

Received 26 June 2001; revised 25 February 2002; accepted 26 February 2002; published 8 November 2002.

[1] Collocated aircraft observations of microstructure and radiative properties of winter boundary layer clouds over the East China Sea and the Japan Sea have been carried out in January 1999 within the Japanese Cloud and Climate Study (JACCS) program. The first part of the paper describes the in situ measured microphysical and optical properties for two cases of boundary layer winter stratocumulus clouds, which concern, first, a rather uniform, supercooled water cloud contaminated by aerosols and, second, a highly heterogeneous, mixed-phase stratiform cloud. Using the Polar Nephelometer, a new instrument for measuring, in situ, the scattering phase function of cloud droplets and ice particles, the polluted, continental-type stratocumulus cloud can be optically regarded as a liquid water cloud because the measured scattering phase functions fitted very well with those calculated from Mie theory for the directly measured FSSP size distributions. In mixed-phase cloud, the measured scattering phase function shows that ice particles strongly affect optical properties of the cloud, where large number of liquid water droplets with higher extinction coefficient and asymmetry factor values were converted into a much smaller number of large ice crystals with lower extinction coefficient and asymmetry factor. Furthermore, a quasi-stable liquid-topped cloud layer with precipitating ice particles was noticed; the layer may, first, affect the cloud radiative properties and, second, seriously restrict the interpretation of satellite cloud composition retrievals. *INDEX TERMS:* 0320 Atmospheric Composition and Structure: Cloud physics and chemistry; 0305 Atmospheric Composition and Structure: Aerosols and particles (0345, 4801); 0360 Atmospheric Composition and Structure: Transmission and scattering of radiation; 0394 Atmospheric Composition and Structure: Instruments and techniques; 3359 Meteorology and Atmospheric Dynamics: Radiative processes; *KEYWORDS:* stratocumulus clouds, microphysics, radiative properties, climate

Citation: Gayet, J.-F., S. Asano, A. Yamazaki, A. Uchiyama, A. Sinyuk, O. Jourdan, and F. Auriol, Two case studies of winter continental-type water and mixed-phase stratocumuli over the sea, 1, Microphysical and optical properties, *J. Geophys. Res.*, *107*(D21), 4569, doi:10.1029/2001JD001106, 2002.

1. Introduction

[2] It is now well recognized that boundary layer clouds have a great influence on weather and climate through their effects on the radiative energy budget in the atmosphere (see, among others, *Fouquart et al.* [1989] and *Heymsfield* [1993]). Despite much research devoted to field experiments and subsequent cloud-radiation modelings [see, e.g., *Nicholls and Leighton*, 1986; *Foot*, 1988], the well-documented simultaneous observations of cloud microphysical and optical properties are still insufficient and essential to improve our understanding of the relationship between radiation and the boundary layer clouds, including mixed-phase conditions. For instance, the microphysical processes that determine cloud droplet size distribution in boundary layer clouds are not completely understood [*Raga and Jonas*, 1993a]. In addition, the existence of the so-called solar anomalous absorption [e.g., *Stephens and Tsay*, 1990] have been repeated during the past several decades, and only *Asano et al.* [2000] have recently provided a direct observational evidence which shows no existence of the solar absorption anomaly for maritime water clouds through a careful instrumented-aircraft experiment. Furthermore, so far only a few field experiments have been conducted to assess the microphysical and radiative properties of mixed-phase boundary layer clouds [*Hobbs and Rangno*, 1998], although those clouds cover significant areas of the Earth's surface at high and middle latitudes in winter season.

[3] During January 1999, intensive aircraft field observations of clouds and radiation were carried out by the Mete-

[1]Laboratoire de Météorologie Physique, CNRS UMR 6016, Université Blaise Pascal, Clermont-Ferrand, France.
[2]Center for Atmospheric and Oceanic Studies, Tohoku University, Sendai, Japan.
[3]Meteorological Research Institute, Tsukuba, Ibaraki, Japan.
[4]Stepanov Institute of Physics, National Academy of Sciences of Belarus, Minsk, Belarus.

Copyright 2002 by the American Geophysical Union.
0148-0227/02/2001JD001106

orological Research Institute (MRI) within the Japanese Cloud and Climate Study (JACCS) program [*Asano and JACCA/MRI Research Group*, 1994]. The experimental strategy was designed to simultaneously document the radiative and microphysical properties of wintertime boundary layer clouds, including mixed-phase situations, by synchronized formation flights with two aircraft. An instrumented Cessna 404 Titan aircraft (named C404 hereafter) was used for radiation and remote-sensing measurements with flight patterns conducted above the clouds. A Beechcraft B200 Super King Air aircraft (B200) was used for in situ cloud microphysics and radiation measurements with collocated flight patterns conducted into the cloud and below the cloud base.

[4] This paper reports on experiments devoted to the study of two winter boundary layer clouds: one featuring an aerosol-polluted and rather uniform stratocumulus water cloud and the other featuring an inhomogeneous, mixed-phase stratiform cloud layer. Both of the clouds were caused by outbreaks of the continental cold air masses over the sea. The results are attempted to provide some basic information on the structural, microphysical and optical properties with the intention of obtaining some insight into cloud radiative transfer problem and into the inference of cloud composition from satellite information. Subsequent measured visible and near-infrared solar absorption are discussed with details in the companion of this paper [*Asano et al.*, 2002] with the interpretation of the results from a numerical simulation study.

2. Aircraft Instrumentation, Data Processing, and Validation

2.1. Aircraft Instrumentation

[5] The various radiometers and usual meteorological instruments installed on the C404 and B200 have already been thoroughly described in a previous paper [*Asano et al.*, 2000]. We describe here the B200 microphysical instrumentation because it has been implemented since the last experiment done in 1998. The microphysical probes operated by MRI are the following: a Passive Cavity Aerosol Scattering probe (PCASP) manufactured by Particle Measuring Systems Inc. (PMS) for the measurement of the aerosol size-distribution from 0.1 to 3.0 μm diameter; a Forward Scattering Spectrometer Probe (PMS FSSP-100) for the sampling of the droplet size-distribution from 3 to 45 μm diameter, a two-dimensional optical array spectrometer (PMS 2D-C) for recording the cloud particle images ranged from 25 to 800 μm diameter and a Gerber Particulate Volume Monitor (PVM-100) for measuring liquid water content and effective diameter of cloud droplets <50 μm diameter [*Gerber et al.*, 1994]. The data measured by these probes were recorded on Science Engineering Associates system (SEA 200) together with the other data measured onboard the aircraft.

[6] The Polar Nephelometer [*Crépel et al.*, 1997] was also mounted on the B200 during the January 1999 JACCS experiment. We recall that the Polar Nephelometer is a unique airborne in situ instrument that is compatible with PMS canister (for a detailed description of the Polar Nephelometer operation, see *Gayet et al.* [1997]). This instrument measures the scattering phase function of an ensemble of cloud particles (i.e., water droplets or ice crystals or a mixture of these particles from a few micrometers to about 800 microns diameter) that intersect a collimated laser beam near the focal point of a paraboloidal mirror. The light scattered at polar angles from ±3.49° to ±169° is reflected onto a circular array of 54 photodiodes. The data are recorded by using a specific data acquisition system (MOTOROLA computer) with a sampling rate which can be manually set from 10 s (0.1Hz) to 1 ms (1 kHz) depending on the particle concentration and the aircraft speed. The direct measurement of scattering phase functions enables to recognize particle type (water droplets or ice crystals), to calculate the optical parameters (extinction coefficient and asymmetry parameter), and to retrieve the cloud microphysical properties (particle size spectra, liquid water and ice contents, particle concentration) by the inversion method developed by *Oshchepkov et al.* [1993]. The sensitivity of the Polar Nephelometer allows one to detect ice crystals as small as a few microns in diameter.

2.2. Methods of Data Processing of PMS Probes

[7] Most of the processed parameters (including microphysics, radiation, thermodynamic and aircraft positioning) were reduced to 1 Hz sampling frequency, which corresponds to a spatial resolution of about 80 m according to the mean cruising speed of the B200.

[8] Corrections for dead time of the FSSP and particle coincidence in the laser beam, as suggested by *Baumgardner et al.* [1985], have been applied to the measured droplet concentrations. No correction to the sizing has been applied. In order to validate the method, liquid water content (*LWC*) and effective diameter (*Deff*) derived from both the FSSP and PVM-100 probes have been compared in water cloud portions in order to avoid FSSP data contamination by ice particles [*Gayet et al.*, 1996a]. The results displayed in Figures 1a and 1b and show quite good agreement characterized by linear relationships and rather low scattering of data points for the two considered parameters. Liquid water content measurements agree to within 20%, whereas a slight systematic difference as much as about 1 μm was found in *Deff* measurements. However, these uncertainties are well within the usual probe accuracies reported [*Baumgardner*, 1983].

[9] The method of 2D-C data processing used in this study has been already described in a previous paper [*Gayet et al.*, 1996b]. A reconstruction technique of the truncated images has been implemented by *Renault* [1998] in order to extend the size range measurement up to 2 mm. Irregular ice particles were the most predominant crystal shape sampled in the present mixed-phase cloud, therefore, the bulk parameters were calculated assuming the following surface-equivalent diameter relationships [*Gayet et al.*, 1993]:

$$d^{eq} = 0.935\ A^{0.5} \qquad (A < 0.049\ mm^2), \tag{1}$$

$$d^{eq} = 0.560\ A^{0.32} \qquad (A > 0.049\ mm^2). \tag{2}$$

For these empirical relations, d_i^{eq} are expressed in millimeter and A_i in millimeter squared. The accuracy of derived microphysical parameters from 2D-C data is given by *Gayet et al.* [1993] and *Larsen et al.* [1998].

2.3. Method of Data Processing of the Polar Nephelometer Measurements

2.3.1. Data Processing and Validation

[10] The data reduction of the Polar Nephelometer measurements consisted, first, in calculating the mean values of

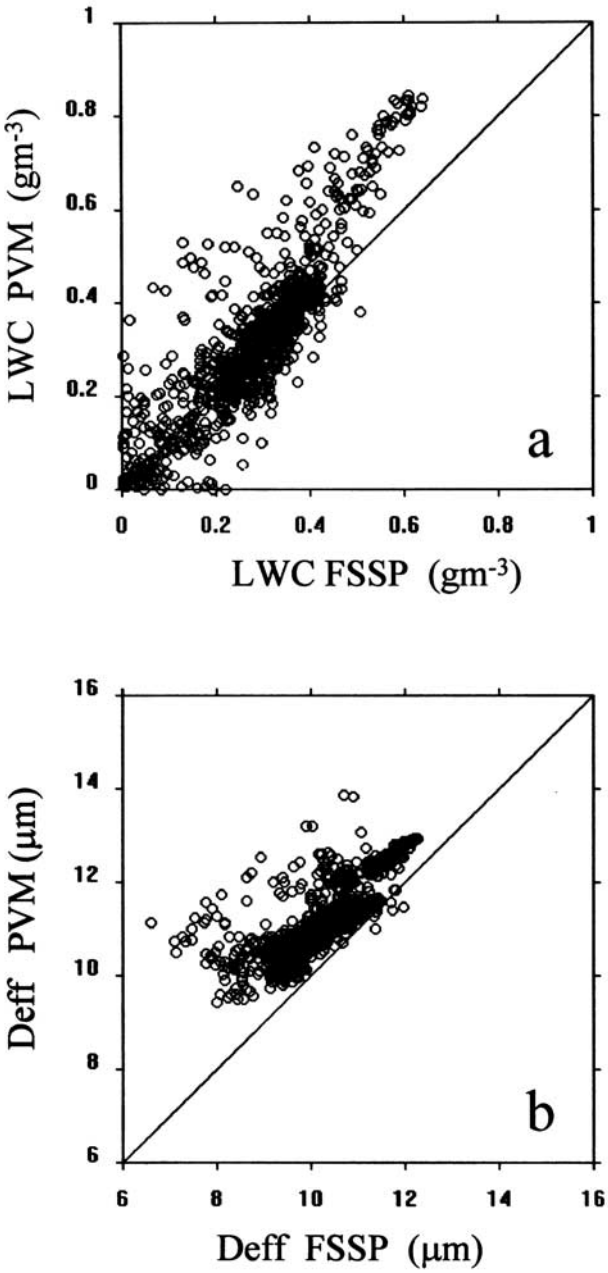

Figure 1. Comparison between Gerber PVM-100 and PMS FSSP probes for the stratocumulus cloud observed on 21 January 1999. (a) Liquid water content. (b) Effective diameter.

the calibrated scattering phase functions over a 1-s interval, then in synchronizing the measurements with the aircraft data recorded on the SEA200 system. The offsets of each recorded channel were estimated from data during clear air sequences; then they were substracted from the corresponding signals. It should be noticed that the Polar Nephelometer measurements at small forward scattering angles ($\theta < 15°$) were not available due to the diffracted light pollution caused by the edges of holes which are drilled on the paraboloidal mirror [*Gayet et al.*, 1997].

[11] In order to validate the Polar Nephelometer measurements the microphysical parameters retrieved from the scattering phase function [*Oshchepkov et al.*, 1993] have been compared with those derived from the size distribution measurements by the PMS FSSP-100. An example result is displayed in Figure 2. The right panel shows the mean scattering phase function measured by the Polar Nephelometer (open circle symbols) during a 20-s sampling in the water-droplet cloud observed on 21 January 1999. In this figure is superimposed the scattering phase function calculated from Mie theory (line) for the FSSP measured droplet size distributions averaged over the same sampling period. Note that the contribution of the droplets larger than 50 μm detected by the 2D-C probe are not significant for the scattering phase function due to the very low concentration of those particles shown in the left panel of Figure 2 (histograms of the corresponding measured FSSP and 2D-C size spectra). The right panel shows that the measured scattering phase function agrees very well with the calculated one. In particular, the scattering phase function at forward angles near $\theta \approx 15°$ and at side angles near $\theta \approx 100°$ is correctly measured, indicating that the illuminating beam has been properly dumped, and reflections of the forward scattered radiation are minimized. Furthermore, the rainbow feature near 140° is correctly measured. In the left panel of Figure 2 the droplet size spectrum (curve) is superimposed that was retrieved by the method of *Oshchepkov et al.* [1993]. Compared to the direct size spectra measured by the FSSP and 2D-C, the retrieved size spectrum agrees very well for mode size and spreading. The results are summarized in Table 1 and show the excellent agreement. In order to confirm the consistency of the results, we extended the comparison to available variation ranges of parameters experienced during the water cloud sampling. Figures 3a to 3d display the retrieved microphysical parameters (droplet concentration, liquid water content, mean volume diameter and effective diameter) versus the direct FSSP measurements. The results confirm that the retrieved parameters agree very closely with the direct parameters over the available dynamical range, highlighting the reliability of the airborne version of the Polar Nephelometer for measuring the scattering phase function.

2.3.2. Extinction Coefficient and Asymmetry Parameter

[12] The derivation of extinction coefficient and asymmetry parameter requires the integration of the scattered light over the scattering angle from 0° to 180°. With the present version of the Polar Nephelometer, the integration of the measurements is impractical for the nearly forward and backward directions (see section 2.3.1). Consequently, we propose two methods to assess the considered parameters.

2.3.2.1. Extinction Coefficient

[13] Assuming randomly oriented non-absorbing particles, we can derive the extinction coefficient (σ_{ext}) with the two following relationships [*Auriol*, 1998]:

$$\sigma_{\mathrm{ext}} = \sum_i Q^{\mathrm{i}}_{\mathrm{ext}} N_{\mathrm{i}}\, A_{\mathrm{i}} \qquad = 2\pi \int_0^{\pi} \Psi(\theta)\sin(\theta)\, d(\theta) \qquad (3)$$

with Q^i_{ext} the visible extinction efficiency (assumed to have a value equal to 2.0 in the range of measured sizes, i.e., large particle approximation), N_i the concentration of particle having a surface A_i, and $\Psi(\theta)$ the volume scattering cross-

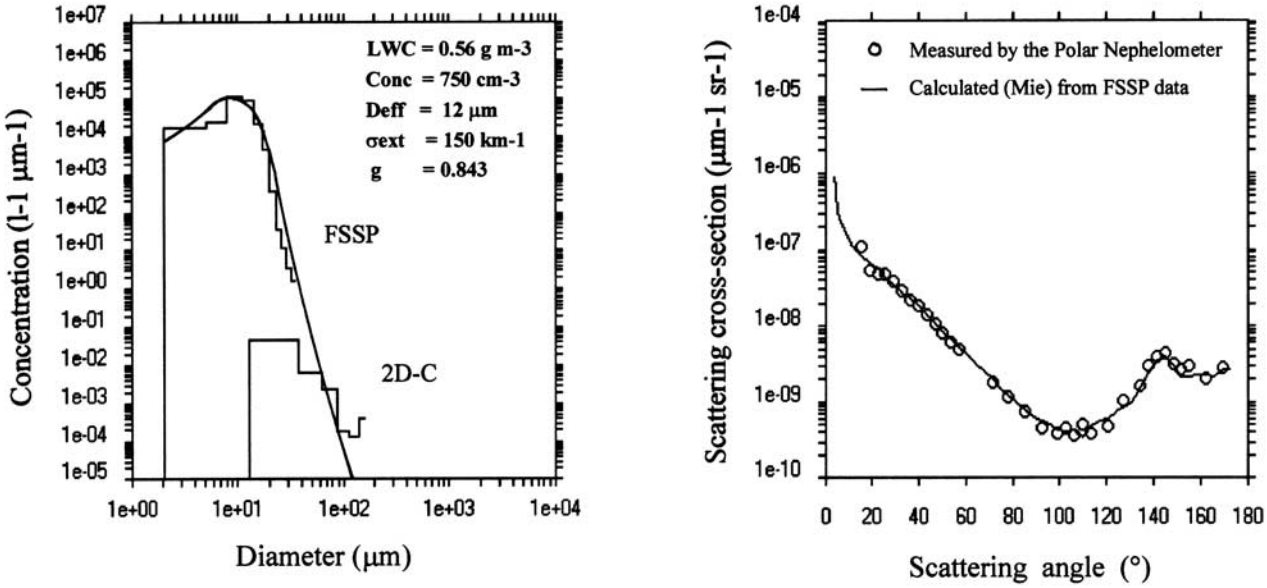

Figure 2. Comparison between Polar Nephelometer and FSSP probe data obtained in water cloud droplets sampling of 20 s duration for the stratocumulus cloud observed on 21 January 1999. (left) Direct FSSP and 2D-C size-distributions (histogram representation) and retrieved droplet size spectrum (curve) obtained by using the inverse-method of *Oshchepkov et al.* [1993] from the measured scattering phase function. Also are reported the mean values of the pertinent microphysical and optical parameters (*LWC*, liquid water content; *Conc*, cloud droplet concentration; *Deff*, effective diameter; *C2D*, ice particle concentration; *IWC*, ice water content; σ*ext*, extinction coefficient; *g*, asymmetry parameter). (right) Mean scattering phase function measured by the Polar Nephelometer (open circle symbols) and scattering phase function obtained by Mie theory (line) calculated with the average droplet size distribution measured by the FSSP over the same time period.

section measured at the scattering angle θ. Assuming now that the integral from 0 to π is proportional to the integral from 15° to 155°, then

$$\sum_i Q^i_{ext} N_i \, A_i \propto 2\pi \int_{15^\circ}^{155^\circ} \Psi(\theta) \sin(\theta) \, d(\theta) \qquad (4)$$

[14] Therefore we have experimentally determined the relationship between the extinction coefficient derived from the PMS measurements (left term of equation (4)) and relative values from the integral (from 15° to 155°) of the volume scattering cross-section measured by the Polar Nephelometer (right term of equation (4)). The results displayed in Figure 4 concern the measurements obtained during cloud segments where only cloud droplets were sampled by the FSSP probe. A linear relationship with a slope parameter of 0.222 and a correlation coefficient of 0.97 were obtained for this case. Therefore, the accuracy of the σ_{ext} derivation from the Polar Nephelometer measurements may be estimated to 25% according to the usual PMS FSSP probe accuracy [*Baumgardner*, 1983]. In this study, the above relationship is assumed to be valid even for ice particles and for a mixture of water droplets and ice particles (mixed-phase).

2.3.2.2. Asymmetry Parameter

[15] The asymmetry parameter (*g*) has been determined according to the method of *Gerber* [1996] and *Gerber et al.* [2000]. The method assumes that the diffraction and refraction components of the scattered light at small scattering angles θ < 15° can be separated. The subsequent ratio *f* of the diffracted portion of the scattered light to the total scattered light has been determined for non-absorbing large spheres to be *f* = 0.56 by using Mie calculations and by assuming typical measured water droplet spectra. In order to assess the accuracy of the method, the *g*-values thus estimated from the scattering phase functions for water droplet cloud segments have been compared with those calculated by Mie theory for the corresponding FSSP mean droplet size-spectra. The comparison shows that the discrepancies of the *g*-values deduced from the Polar Nephelometer measurements are smaller than 2%.

[16] Without any a priori information of water phase of cloud particles, the value of *f* = 0.56 is assumed even for ice particles. In fact, this value is close to the average value that can be estimated from the theoretical results of *Takano and*

Table 1. Comparison Between the Directly Measured (FSSP) and Retrieved (Polar Nephelometer) Microphysical Parameters for the Stratocumulus Cloud Observed on 21 January 1999[a]

Parameter	FSSP Values	Retrieved Values	Relative Discrepancies
Conc, cm^{-3}	750	780	4.4%
LWC, g/m^3	0.56	0.64	15.3%
Dm, µm	10.4	10.5	−0.5%
Deff, µm	12.0	13.0	13.9%

[a] *Conc*, droplet concentration; *LWC*, liquid water content; *Dm*, mean diameter; *Deff*, effective diameter.

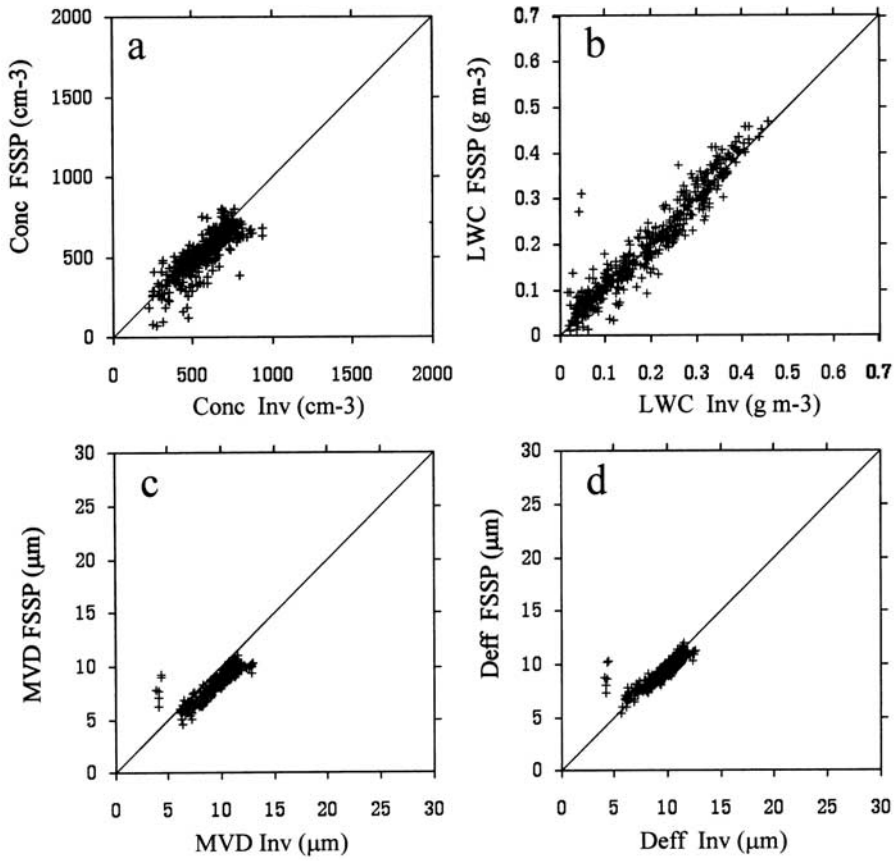

Figure 3. (a–d) Comparison of direct (FSSP) and retrieved (Polar Nephelometer) microphysical parameters (Conc, cloud droplet concentration; LWC, liquid water content; MVD, mean volume diameter; Deff, effective diameter). The results concern the water droplet cloud sequence for the stratocumulus cloud observed on 21 January 1999.

Liou [1989, 1995] obtained for a variety of ice crystal shapes. Nevertheless, due to deficiencies in theoretical approaches, particularly for irregularly shaped ice crystals, significant uncertaincies may remain in the *g*-value determination, but the relative fluctuations of this parameter probably reflect the actual cloud optical properties.

3. Microphysical and Optical Properties of Two Cases of Boundary Layer Clouds

[17] The flight pattern strategy used in the field experiment was the same as that previously described in details by *Asano et al.* [2000]. At the start of the experiment, the B200 performed in situ measurements of cloud microphysical structures at several flight levels in the cloudy layer. Then, the B200 flew below the cloud layer with a synchronized flight formation with the C404 (flying above the cloud) in order to measure the solar radiation budget due to the cloud layer.

3.1. Water Droplet Stratocumulus Case (Flight on 21 January)

3.1.1. Meteorological Situation

[18] The observation presented in this section was carried out on 21 January 1999 (between 11:10 and 13:30 JST) in an area of 70 km × 70 km centered at 32.2°N and 129.5°E, located about 100 km west of Kyûshû island. On that day a typical winter-type pressure pattern with a high pressure system widely covered the East China Sea. There was an outbreak of cold air mass from the east Asian Continent, which caused an extensive stratocumulus layer over the southern part of the East China Sea as revealed from the visible image taken by GMS-5 satellite (Geostationary Meteorological Satellite 5) at 00UT (09 JST) around the region. Over the observational area, the vertical profiles (see below) reveal that the cloud was about 500 m deep with a cloud-layer base near 1000 m, a temperature of −2.5°C and a cloud-top height at 1500 m with a temperature of −6°C. The cloud was topped by a strong temperature inversion as much as 5°C, and the atmosphere over the cloud layer was clear and dry with relative humidity below 10%. Visual observations from the aircraft revealed a rather uniform cloud field.

3.1.2. Microphysical and Optical Parameters

[19] In this section we discuss the vertical profiles of several pertinent microphysical and optical parameters obtained during the descent flight pattern by the B200 in the cloud layer between 11:30 and 12:20 (Figures 5a to 5i), for which four sampling sequences of each about 12-minutes duration were performed at distinct levels of 500, 200, 350 and 100 m above the cloud base. Obviously, the cloud parameter values must be considered only as estimates because of the natural cloud inhomogeneities, the cloud time-variability and the different geographical locations of the aircraft during the corresponding flight sequences. For

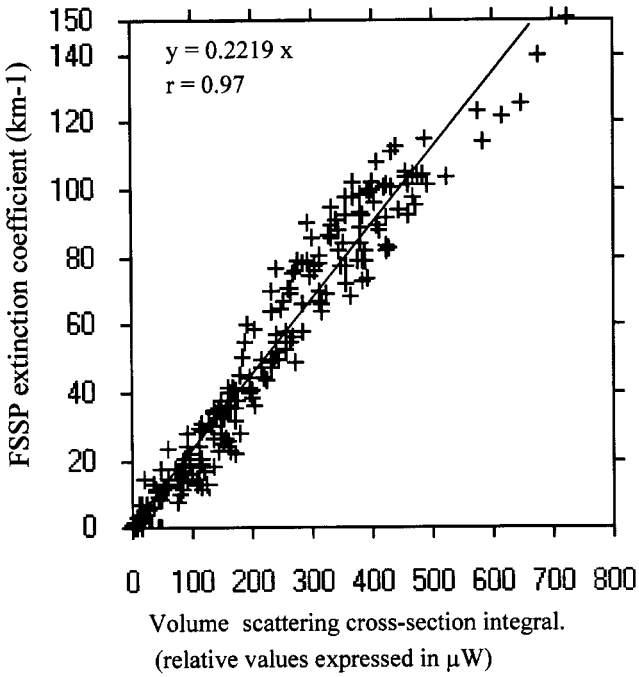

Figure 4. Visible extinction coefficient derived from the FSSP measurements versus the relative values from the integral (from 15° to 155°) of the scattering cross-section measured by the Polar Nephelometer.

instance, in Figure 5, the large variability of the parameters at the four levels considered reveals the cloud horizontal heterogeneities. Nevertheless, these vertical profiles obtained during the 50 minutes duration are rather well correlated in magnitude with other three profiles derived from B200 ascent-descent sequences carried out at the beginning and during the second part of the flight (13:00–13:30).

3.1.2.1. Cloud Microstructure

[20] The aerosol-number concentration derived from the PCASP measurements (Figure 5a) shows that the aerosol concentration was around 1200 cm^{-3} below the cloud base (with peak values up to 1500 cm^{-3}, not represented in Figure 5a), and then it dropped down to 150 cm^{-3} at the cloud base level. The mean diameter of aerosol particles was about 0.15 μm (in the range of the PCASP measurements), but nothing is known about the aerosol composition. The cloud droplet-number concentration exhibits a rather constant maximum value (≈1000 cm^{-3}) with height (Figure 5b), whereas the effective diameter increases with the cloud altitude from 6 to 12 μm (Figure 5c). These cloud properties obtained over the East China sea reveal rather polluted air-mass characteristics and point out that this situation would not necessarily be of maritime-type as also reported by *Raga and Jonas* [1993b] from observations over the sea around the United Kingdom. A back trajectory analysis suggests that the northwesterly wind at the cloud levels might load continental (polluted) air mass from the Northeast Asian continent.

[21] The liquid water content (*LWC*) mainly increases with height up to 0.65 g/m^3 at the cloud top (Figure 5g). While the peak measured values of *LWC* at three of the four level flight legs agree with estimated adiabatic *LWC* most of the measured values of *LWC* are seen to be smaller. This suggests that only occasionally were small portions of cloud adiabatic, while on the average the cloud consisted of subadiabatic *LWC*. This feature is mainly caused by vigorous entrainment processes rather than fractional cloudiness because of its rather high value (~80%).

[22] Ice particles have been found at every levels of the cloud layer with very low concentrations (i.e., a few per liter up to 20 l^{-1}; see Figure 5e). They were mainly composed of rimed columnar crystals as shown in Figure 6 with the largest size measured near the cloud base (Figure 5f). Subsequently, only traces of the ice water content were detected (Figure 5d). A few drizzle drops have also been detected below the cloud base, which probably resulted from melting of ice particles. The non-precipitating feature of the layer cloud is consistent with the polluted, continental-type situation. Due to the small size of cloud droplets the collision-coalescence process was rather ineffective, reducing drastically the drizzle formation and the formation of high ice particle concentrations by both primary and secondary processes [*Hobbs and Rangno*, 1995].

3.1.2.2. Optical Characteristics

[23] The liquid water path (*LWP*) deduced from the *LWC* profile shown in Figure 5g gives a value of about 165 g m^{-2} which is close to the mean *LWP* value (215 gm^{-2}) measured with the nadir-looking microwave radiometer operated at 31.4GHz onboard the C404 (see the *LWP* frequency distribution shown in Figure 7). The extinction coefficient profile ($\sigma_{ext,}$) inferred from the Polar Nephelometer is displayed in Figure 5h, and it exhibits a monotonic increase up to 160 km^{-1} near the cloud top; the profile leads to a visible optical depth (τ) of about 40. The asymmetry parameter in Figure 5i monotonically increased with the effective diameter (see Figure 5c) from about 0.830 near the cloud base to 0.845 at the cloud top. These values are typical of water cloud [see, e.g., *Raga and Jonas*, 1993b] and highlight that the presence of ice particles mentioned above has not significantly affected the cloud optical properties.

[24] *Foot* [1988] showed that for optically thick clouds, their radiative properties are dominated by the microphysical characteristics in the top 100 m depth or so of the clouds. In Figures 8a and 8b are displayed the relative frequencies of the *g*-values and extinction coefficients measured during the flight sequence performed near the cloud top. The figures clearly show single-mode distributions with mean values of 0.836 and 82 km^{-1}, respectively. The dispersion of the distributions and the subsequent standard deviations (0.004 and 30 km^{-1}, respectively) may characterize the heterogeneities of the optical properties that characterize the stratocumulus layer top. Furthermore, Figure 9 shows a typical example of the Polar Nephelometer measurement sampled very close to the cloud top, which highlights that the cloud layer can be optically regarded as liquid water cloud because the measured scattering phase function agreed very well with those calculated by Mie theory from the corresponding FSSP size distribution.

3.2. Mixed-Phase Stratocumulus Case (Flight on 30 January)

3.2.1. Meteorological Situation

[25] The mixed-phase stratocumulus cloud was observed on 30 January 1999 between 10:50 and 13:20 local time in

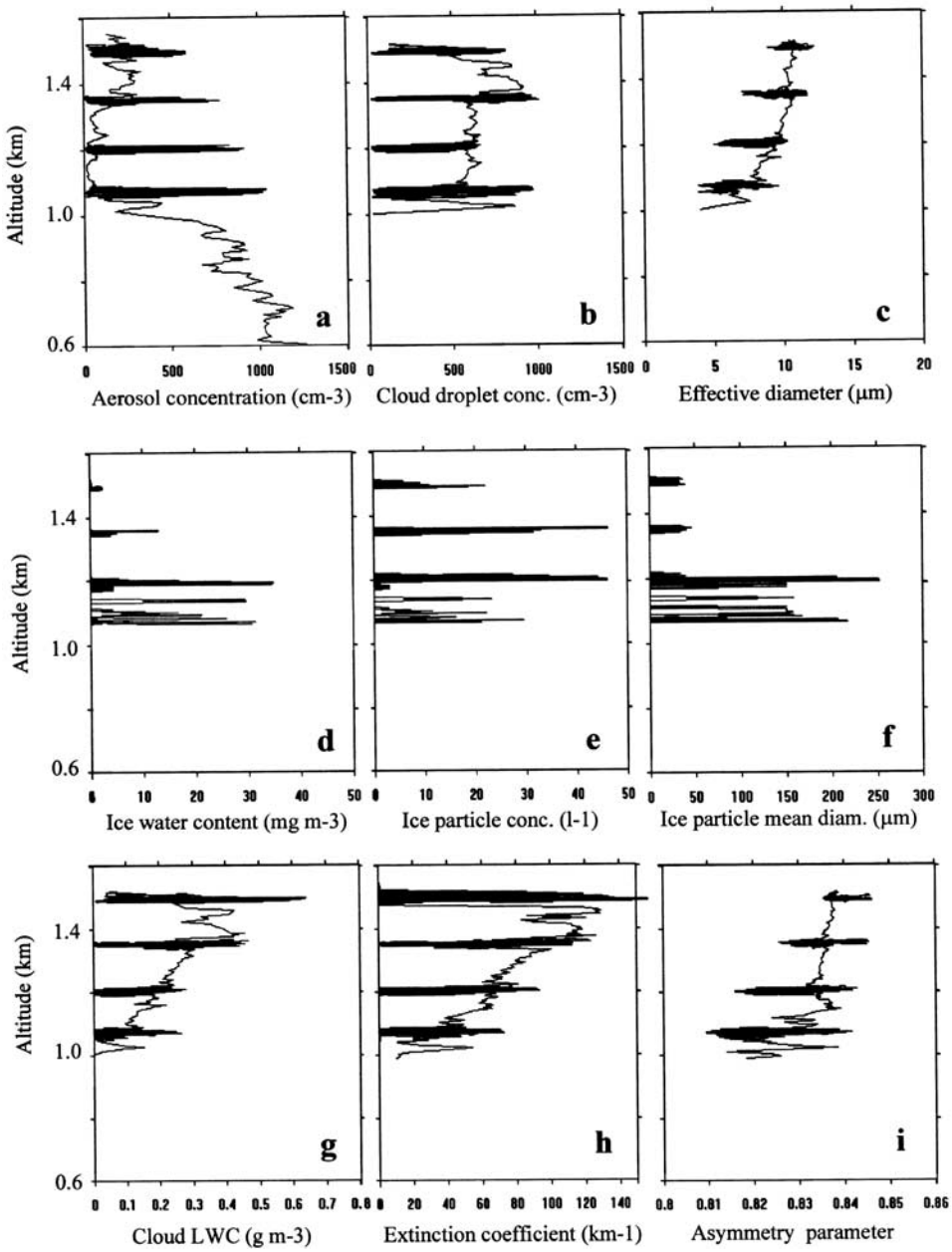

Figure 5. Vertical profiles of microphysical parameters relative to the 21 January stratocumulus case study: (a) aerosol concentration, (b) cloud droplet concentration, (c) effective diameter, (d) ice water content, (e) 2D-C particle concentration, (f) 2D-C mean particle diameter, (g) liquid water content, (h) extinction coefficient and (i) asymmetry parameter.

an area of 50 km × 50 km centered at 35.9°N and 135.4°E, north of the Wakasa bay. From 29 January through the early morning of 30 January, there were intermittently heavy snowfalls in the regions facing the Japan Sea of the western parts of Japan Islands. On that day the winter-type pressure pattern began to weaken with a moving high-pressure system from west. During the observation, the Wakasa bay area was still covered by multilayered stratocumulus clouds as revealed from the visible image taken by GMS-5 satellite at 02UT (11JST). At the beginning of the experimental flight, the cloud top looked rough and fluffy with many domes and hollows. We often observed the optical phenomena of sub-sun and glory from the C404 flying above the clouds, this indicates that the cloud layer, so called mixed-phase cloud, contained water droplets as well as ice particles. However, at the end of the observation the cloud top was getting flat, indicating that the stratocumulus cloud system developed towards a decaying stage. The cloud layer was about 1300 m deep; the top was at about 2300 m with a mean temperature of −15°C, and the cloud base was near 1000 m with −7°C. Above the cloud top, the atmosphere was clear and dry. On the other hand, there were still occasional snowfalls below the cloud layer.

3.2.2. Microphysical and Optical Parameters

[26] Similarly to the previous water cloud case, Figures 10a through 10i display a composite representation of

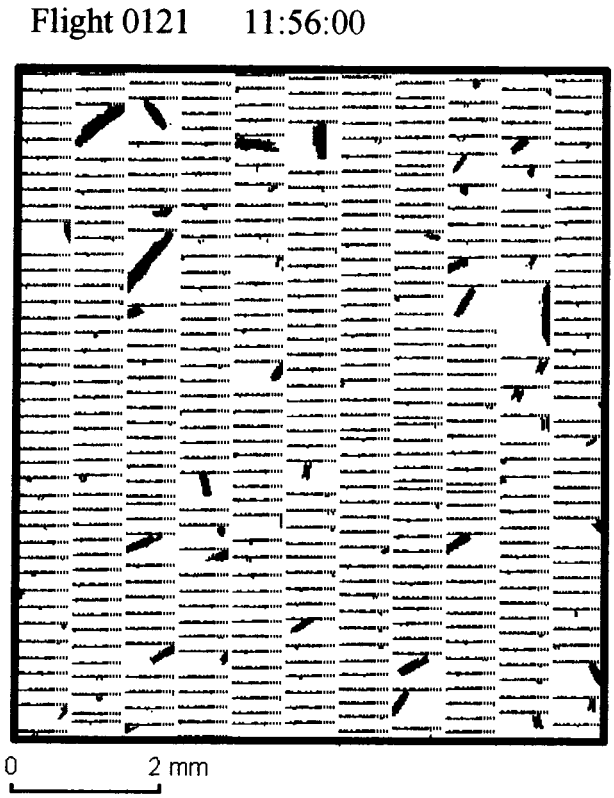

Figure 6. Example of ice particles sampled by the 2D-C probe at 1200 m MSL/−4°C in the stratocumulus cloud observed on 21 January 1999.

vertical profiles for pertinent microphysical and optical parameters obtained during the B200 ascent in the cloud layer between 10:55 and 11:40 (JST), for which four sampling sequences were also included at discrete levels of 100, 600, 1100, and 1300 m above the cloud base. Compared with the previous water-cloud case, the representativeness of the vertical profiles shown in Figure 10 is much more problematic due to the higher degree of horizontal and vertical heterogeneities for all of the considered parameter. Here, the cloud microstructure, ice phase and optical characteristics are discussed keeping in mind that the results in Figure 10 do not represent an instantaneous cloud vertical profile.

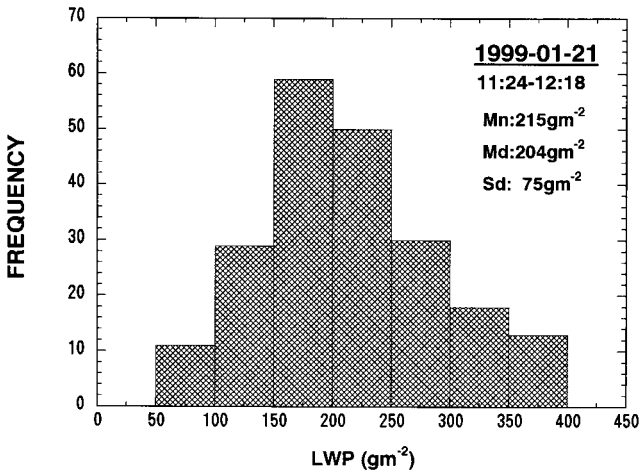

Figure 7. Histogram of the liquid water path (*LWP*) derived from nadir microwave radiance measurements (C404). *Mn*, *Md* and *Sd* are the mean value, the median value and the standard deviation, respectively. 21 January case study.

3.2.2.1. Cloud Microstructure

[27] The vertical profile of aerosol number-concentration in Figure 10a derived from the PCASP measurements shows that in the sub-cloud layer the average aerosol concentration (350 to 400 cm^{-3}) is much lower than that characterizing the previous case; the concentration then dropped down to 10 cm^{-3} near the cloud base level. The mean diameter of PCASP measured aerosol particles was 0.2 μm in the sub-cloud layer. In the first lower half of the cloud depth, the

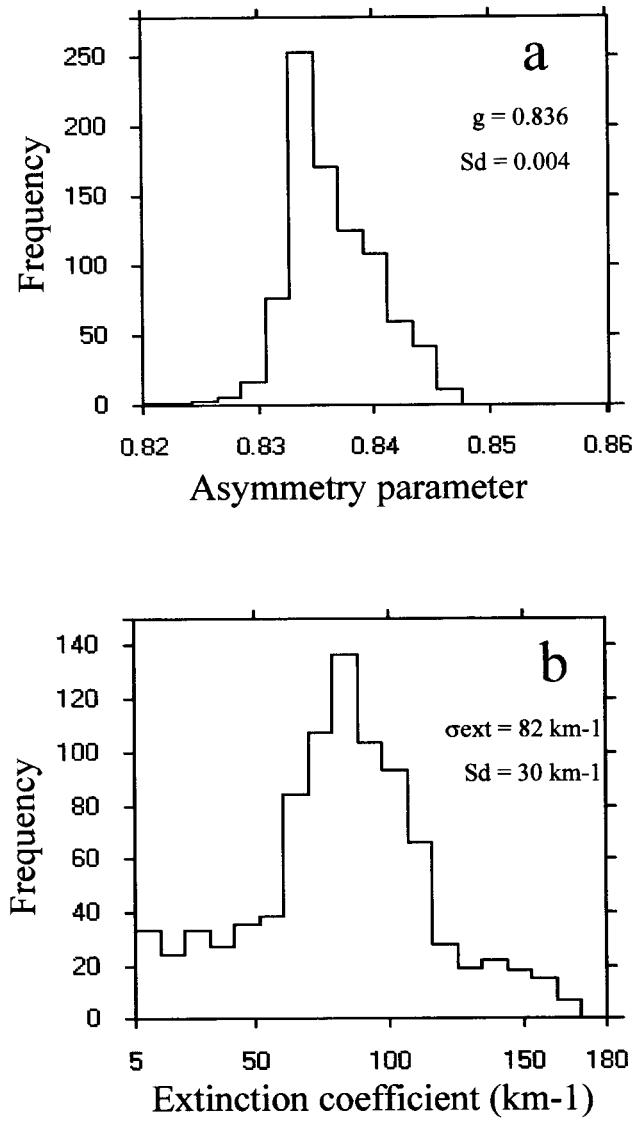

Figure 8. Frequency distributions measured near the cloud top of (a) asymmetry parameter and (b) extinction coefficient. The mean value and standard deviation are reported. 21 January case study.

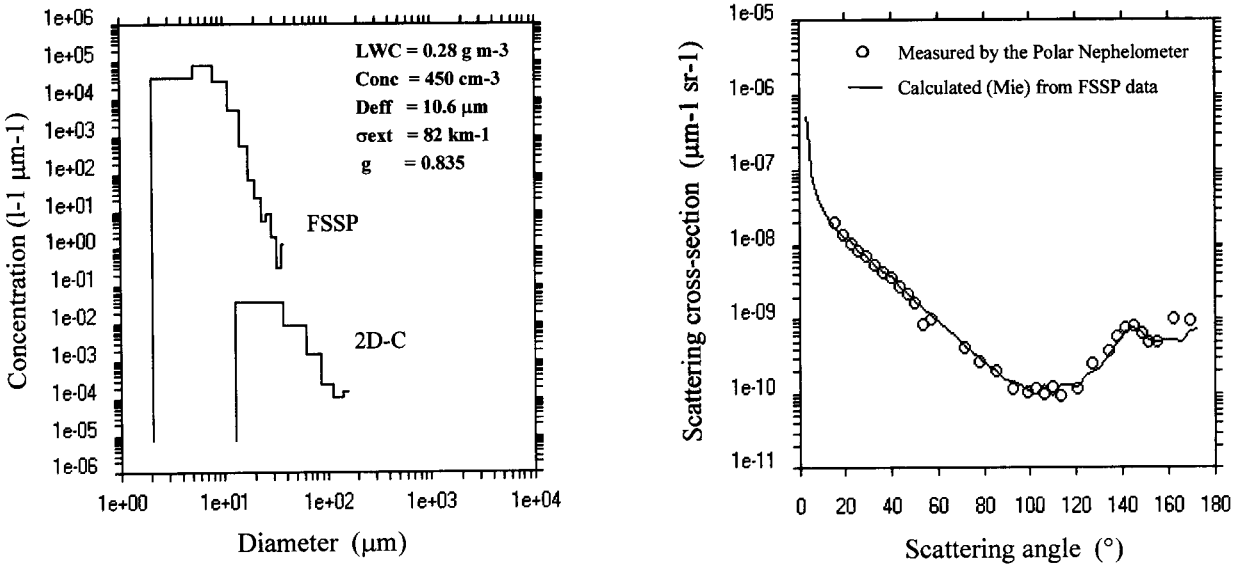

Figure 9. Same as Figure 2, but for the measurement near the cloud top at 1500 m (MSL) with a temperature of −6°C. 21 January case study.

cloud droplet concentration measured by the FSSP reached 300 to 400 cm^{-3} (Figure 10b), and the effective diameter increased with the cloud altitude from 10 to 16 μm (Figure 10c). Despite the cloud situation over the sea, these characteristics are rather similar to the continental stratus clouds reported by *Sassen et al.* [1999]. The back trajectory analysis suggests that continental air mass with northerly wind at the cloud levels might come from east of Siberia.

[28] The *LWC* profile in Figure 10g indicates vertical cloud heterogeneities with a largest *LWC* value of 0.4 g/m^3 measured 300 m above the cloud base. From the results in Figure 10, it is obviously not possible to identify a well-defined multilayered aspect of the present cloud case. The thermodynamical sounding reveals a water-saturated layer within the cloud depth with a temperature decrease that is very near the pseudo-adiabatic lapse rate in the cloud layer. In addition, the vertical profiles obtained during the B200 ascent and descent flight sequences revealed peaks and/or traces of liquid water, which were observed at any level in the cloud depth. The *LWC* profile in Figure 10g also shows a significant remnant (up to 0.1g/m^3) of liquid water in the top of the cloud; this is an important feature that will be discussed later in detail. The subsequent cloud droplet concentration decreased to 100 cm^{-3} with an effective diameter that exhibits large variations between 7 and 15 μm.

3.2.2.2. Ice Phase

[29] In contrast to the vertical profile of the liquid-water cloud droplets, ice particles were observed at any cloud level and below the cloud base (snowfall) from the 2D-C probe measurements (see profiles in Figures 10d to 10f). The mean characteristics of ice particles can be summarized as follows: the ice water content (*IWC*) in Figure 10d ranges from 0.1 to 0.4 gm^{-3}. These values, compared to the maximum *LWC* measured in the same cloud layer, denote an efficient water-ice conversion rate leading to heavy mixed-phase conditions. The ice particle concentration (Figure 10e) was rather low near the cloud top (≈20 l^{-1}) and reached 200 l^{-1} near 1300 m MSL at −8°C. The mean ice-particle size remained fairly constant through the cloud depth as shown in Figure 10g. These characteristics are consistent with the observational results by *Hobbs and Rangno* [1985] for various types of stratiform clouds. Dominant ice-crystal types just below the cloud top were pristine dendritic, and assemblage of dendritic particles were also observed in some places, with maximum dimension up to 2 mm, as exemplified in Figure 11. Most of these crystals must have originated in the cloud top layer, since only in the upper most part of the cloud, the temperature could attain as low as to −15°C, around which dendrites can begin to grow. It should be noticed that the 2D-C probe is unable to detect small fresh-nucleated ice crystals until they had grown to size larger than about 25 μm. Branched ice particles resulted from a rapid growth rate in a supersaturated air with respect to ice might cause a subsequent rapid depletion of the cloud water droplets (Findeisein-Bergeron process), explaining the observed inhomogeneous *LWC* profiles. Rimed dendritic crystals and graupel-like particles were observed in the active cloud parts characterized by the higher *LWC* values. The precipitation below the cloud base was characterized by both large rimed particles and snowflakes. Additionally, no evidence of ice multiplication by splintering [*Hallet and Mossop*, 1974] was detected in this case, simply because the cloud temperature range (−7 to −15°C) did not satisfy the requirement of ice splinter production (−3 to −8°C, *Choularton et al.* [1980]). The above observations for the mixed-phase cloud microstructure, experienced during two hours, suggest a subtle equilibrium between liquid-water droplet production and water removal by ice particles and support the modeled results by *Harrington et al.* [1999] for the stability of cold mixed-phase layers.

3.2.2.3. Optical Characteristics

[30] It is obviously not possible to derive a reliable value of the liquid water path (*LWP*) from the *LWC* profile shown in Figure 10g. However, this information was obtained from the nadir-looking microwave radiometer onboard the C404,

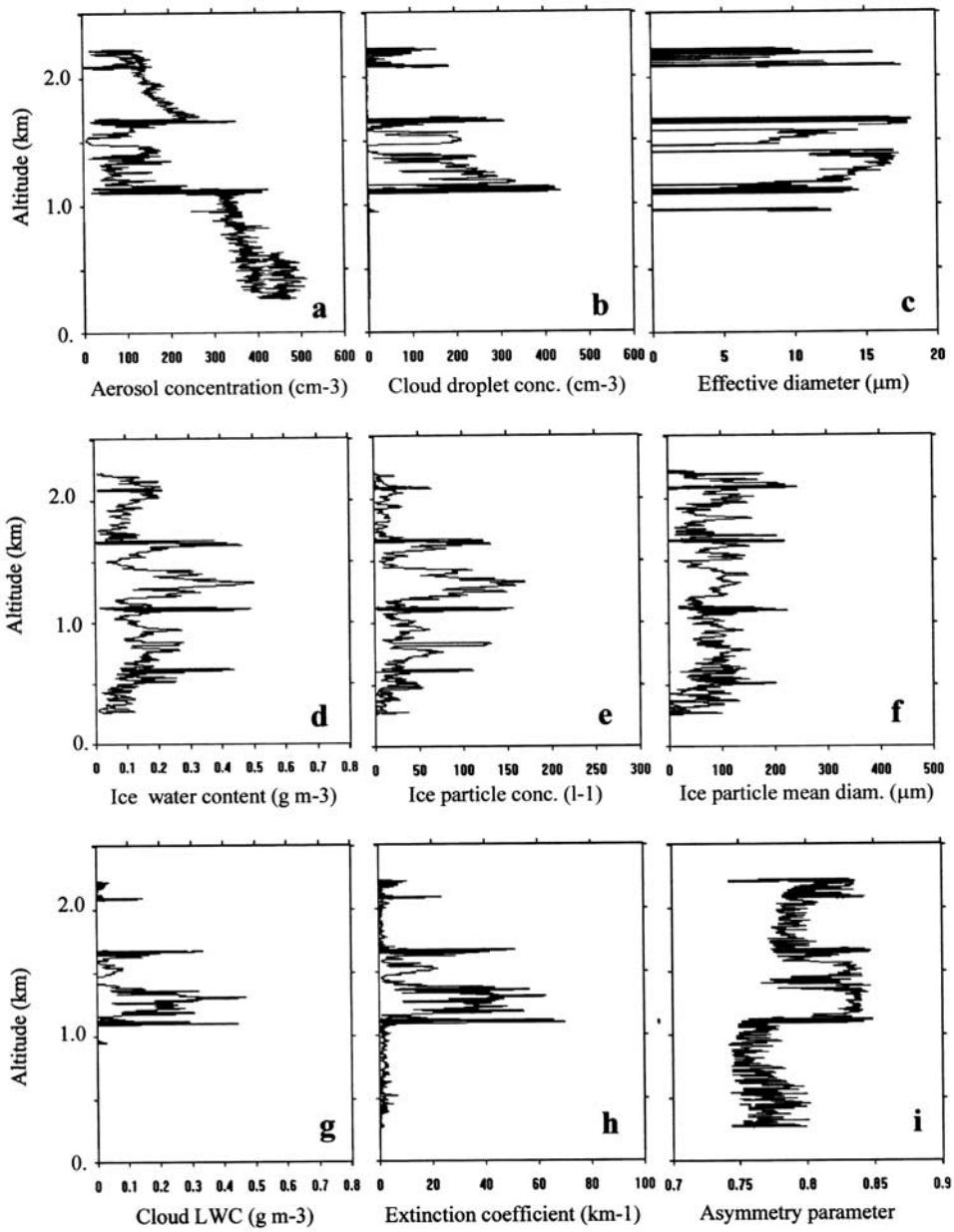

Figure 10. Vertical profiles of microphysical parameters relative to the 30 January 1999 stratocumulus case study: (a) aerosol concentration, (b) cloud droplet concentration, (c) effective diameter, (d) ice water content, (e) 2D-C particle concentration, (f) 2D-C mean particle diameter, (g) liquid water content, (h) extinction coefficient and (i) asymmetry parameter.

which measured a mean *LWP* of 150 gm^{-2} (see *LWP* histogram of Figure 12). Although the mixed-phase stratocumulus was geometrically much thicker than the previous case, the mean *LWP* was significantly lower than the value of the water cloud (215 gm^{-2}, see Figure 7). The maximum value of the extinction coefficient (σ_{ext}) in Figure 10h reaches only 80 km^{-1} (i.e., about one-half of the previous case), and the corresponding cloud optical depth (τ) was roughly estimated to 20. The extinction coefficient (σ_{ext}) profile exhibits large cloud heterogeneities, which are linked to the variations of both *LWC* and asymmetry parameter shown in Figure 10i. In the mixed-phase cloud, the scattering properties were primarily dominated by water cloud droplets, because the *g*-values were ranged from 0.82 to 0.85, which are typical values for water clouds [*Raga and Jonas*, 1993b], and because the larger g-values were linked to the larger values of *LWC*. Smaller *g*-values between 0.73 and 0.80 seem to be related to ice-particle occurrence (see *IWC* profiles in Figure 10d) and to the relatively smaller σ_{ext} values. These *g*-values are within the range of the results estimated from the recent theoretical calculations of the light scattering by ice crystals [e.g., *Macke et al.*, 1998; *Liou et al.*, 2000].

[31] The cloud heterogeneities noted from the variability of the microphysical and optical parameters in both horizontal and vertical scales were confirmed by the nadir-

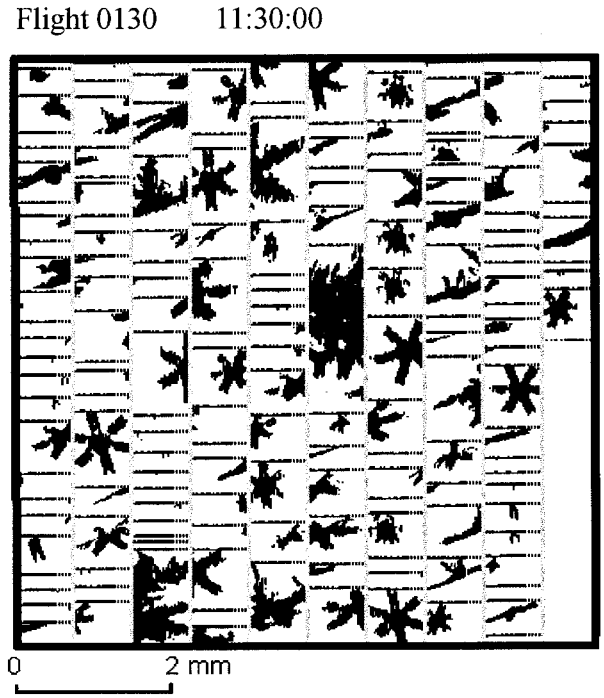

Figure 11. Example of ice particles sampled by the 2D-C probe near the cloud top at 2300 m (MSL) with a temperature of −15°C for the stratocumulus cloud observed on 30 January 1999.

looking infrared radiation measurements with the radiation thermometer onboard the C404. As a matter of fact, the frequency distribution shown in Figure 13 reveals a fairly inhomogeneous cloud top temperature field with a mean value of −14.6°C, which is in accordance with the thermodynamical sounding.

[32] Figures 14a and 14b display, respectively, the relative frequency of the *g*-values and the extinction coefficient measured by the Polar Nephelometer during the near cloud-top flight at 2300 m at temperature −15°C. The mean value of σ_{ext} was rather small of only 10 km^{-1}, compared to 82 km^{-1} for the previous water cloud case. The *g*-distribution exhibits two modes centered around 0.835 and 0.79 and indicates that about 70% of the measurements are characterized by *g*-values (0.82 to 0.85) corresponding to water droplets and about 30% by ice particle values (0.76 to 0.80).

[33] The above results clearly show that the present mixed-phase cloud exhibits a liquid-water topped cloud layer in which ice precipitation was yielded. This feature is likely common with the Arctic clouds studied by *Hobbs and Rangno* [1998], and it may play an important role in cloud radiative properties and remote sensing [*Harrington et al.*, 1999]. Since the scattering properties near the cloud top are mostly dominated by water droplets, the interpretation of satellite remote sensing of mixed-phase clouds (under the assumption of water clouds) may seriously restrict the inference of cloud compositions [*Liou and Takano*, 1994; *Buriez et al.*, 1997; *Riedi et al.*, 2000].

[34] In order to put forward interpretation of these near-cloud top properties, we report a few examples, in Figures 15 and 16, of the scattering properties with two typical *g*-values measured by the Polar Nephelometer measurements. The figures represent the measured phase functions (open circle symbols) for the corresponding particle size-spectra obtained by both the PMS FSSP-100 and 2D-C probes (histograms) and ice particle images sampled by the 2D-C probe (above right corner). Despite the response of the FSSP is unreliable in presence of irregular large ice crystals [*Gayet et al.*, 1996a], we have superimposed in Figures 15 and 16 the scattering phase functions calculated by Mie theory for the measured FSSP mean droplet size-spectra (line), by assuming spherical ice particles.

[35] Figure 15 displays an example of mixed-phase cloud representing cloud composition dominated by water droplets. The close agreement between the two scattering phase

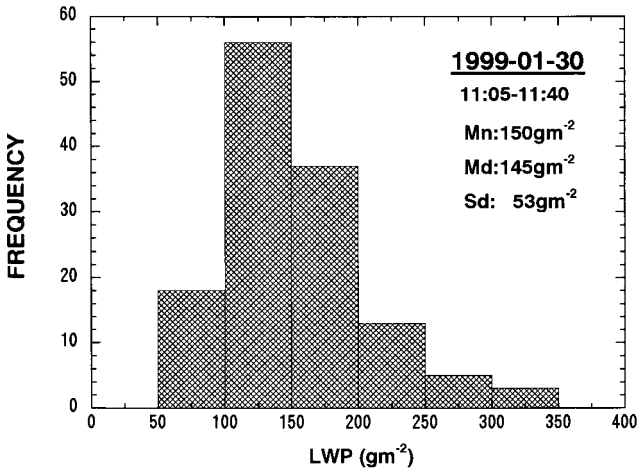

Figure 12. Histogram of the liquid water path (*LWP*) derived from nadir microwave radiance measurements (C404) for the stratocumulus cloud observed on 30 January 1999. *Mn*, *Md* and *Sd* are the mean value, the median value and the standard deviation, respectively.

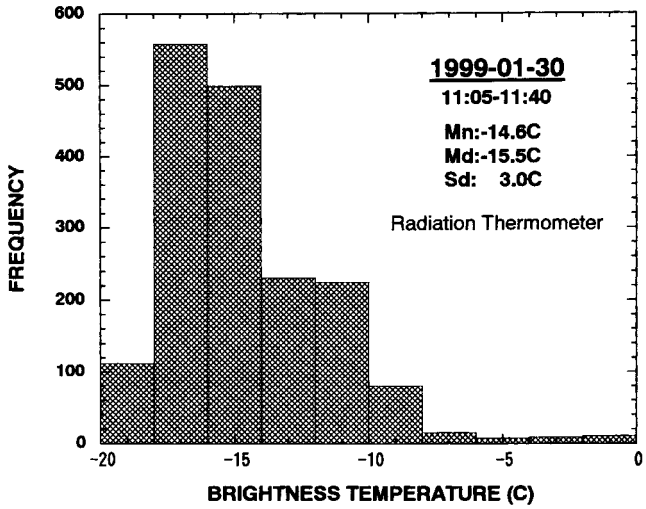

Figure 13. Histogram of the brightness temperature derived from nadir-looking infrared thermometer onboard the C404 for the stratocumulus cloud observed on 30 January 1999. *Mn*, *Md* and *Sd* are the mean value, the median value and the standard deviation, respectively.

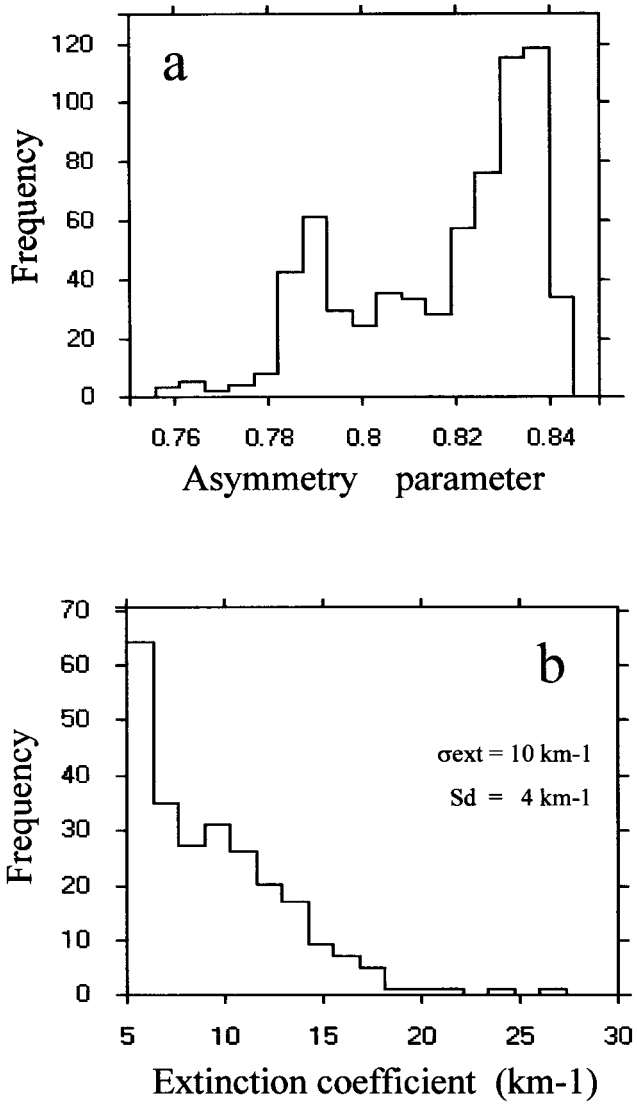

Figure 14. Frequency distributions of (a) asymmetry parameter and (b) extinction coefficient, measured near the cloud top for the stratocumulus cloud observed on 30 January 1999. The mean value and standard deviation are reported.

functions highlights that this cloud portion can be optically regarded as liquid water cloud and that ice crystals did not significantly contaminate the FSSP measurements probably because their concentration was very low ($C2D \approx 0.5\ l^{-1}$, $C2D$ being inferred from the 2D-C probe measurements). This example clearly shows that a small number of cloud water droplets ($Conc \approx 45\ cm^{-3}$, $LWC \approx 10\ mg\ m^{-3}$) near the cloud top dominated the optical properties ($g \approx 0.83$), even though there were pristine dentric-shaped ice crystals having an ice-water content twice-larger than the droplet liquid-water content ($IWC/LWC \approx 2$) and there might be fresh-nucleated, small ice crystals.

[36] Figure 16 shows a typical example of heavy mixed-phase cloud. Compared to the above example, the ice crystals such as pristine-dentric-shaped and some aggregates are characterized by much higher ice-water-content ($0.28\ g\ m^{-3}$) and number concentration ($C2D = 55\ l^{-1}$). Assuming that the FSSP probe measures only water droplets, the comparison of the measured phase function and the theoretically calculated one for the assumed pure water cloud shows that scattering by ice particles is considerably stronger at the side angles between 80 and 120°, leading to a significantly smaller g-value (0.79) than for the scattering by water clouds. For the first time, the results obtained from the in situ measurements have confirmed the findings by *Sassen and Liou* [1979] for the mixed-phase clouds formed in their laboratory experiments. Furthermore, as noticed by those authors, the small bump near 145° on the measured scattering phase function suggests the presence of relatively small amount of water droplets that still contribute to the scattering properties. This feature can be qualitatively confirmed by the FSSP measurements, which evidence a droplet concentration of 15 cm^{-3} and an effective diameter of 5 μm. Subsequently, the contribution of such remnant of water droplets should bring a slight increase of the *g*-value in comparison with the case of pure ice clouds. The two typical examples shown in Figures 15 and 16 confirm that the scattering properties of mixed-phase clouds strongly depend on cloud water-ice balance [*Sassen and Liou*, 1979].

[37] Coming back to Figure 10g, the results show that in precipitating regions, the ice-phase was optically dominant because the *g*-parameter values were rather low, ranging between 0.74 and 0.78. Figure 17 illustrates a typical example of ice dominant clouds measured near the cloud base at 900 m MSL with −6°C. The results show that ice particles (mainly composed of rimed crystals and graupels) lead to a featureless measured phase function with a corresponding *g*-value of 0.76. The ice water content and ice particle concentration were 160 mg m^{-3} and 44 l^{-1}, respectively. The prominent cloud bow near 140° was not observed; this signifies that the smaller particles of less than 45 μm, which might be hypothesized to be water droplets, did not contribute to the scattering properties as confirmed by the theoretical pattern derived from the FSSP-measured size distribution.

4. Conclusions

[38] The present case studies for the two winter boundary layer clouds over the sea exhibit essential differences in both microphysical and optical properties. Those of the rather uniform, supercooled water stratocumulus cloud sampled on 21 January 1999 over the East China Sea were strongly affected by aerosols which were estimated by the back trajectory analysis to be largely dust particles transported long-range from the northwestern, desert area of China. The cloud was characterized by very high aerosol concentrations in the sub-cloud layer and fairly high cloud droplet concentrations. This feature leads the cloud to a polluted, continental-type and non-precipitating structure. The liquid water content and effective diameter increased with height up to very close the cloud top with temperature −6°C. The direct measurement of the scattering phase functions by the Polar Nephelometer has confirmed that the stratocumulus cloud can be optically regarded as liquid water cloud because the measured scattering phase function fitted very well with those calculated by Mie theory for the direct FSSP-measured size distributions.

[39] The microphysical and optical properties for the mixed-phase stratocumulus cloud sampled on 30 January

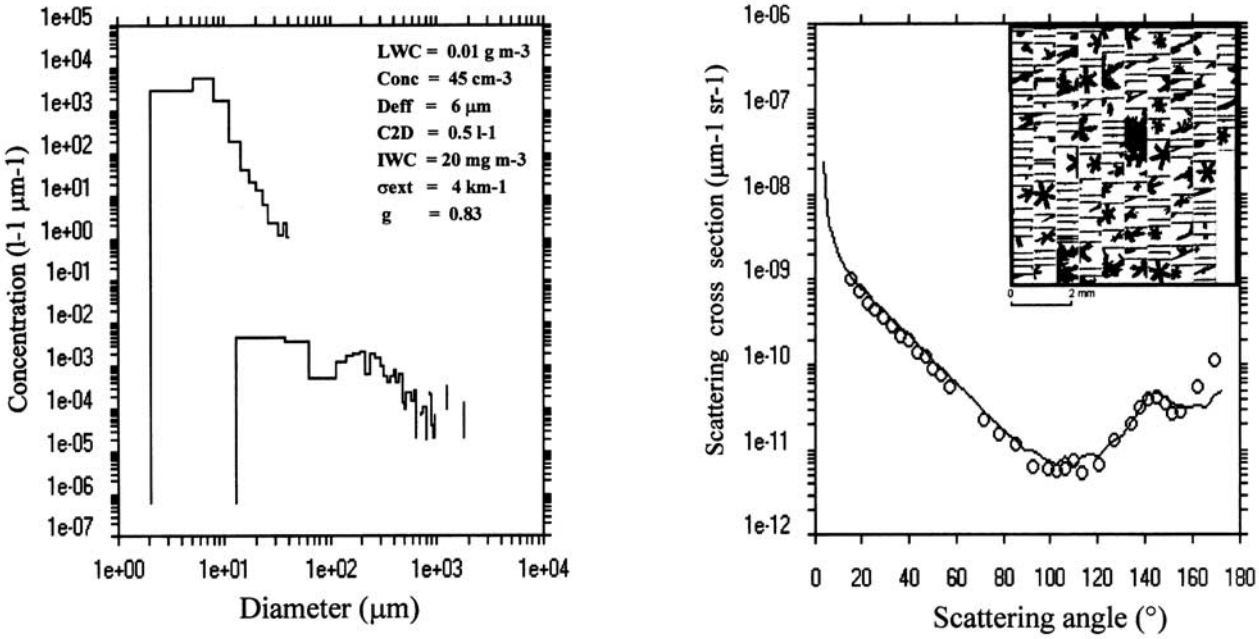

Figure 15. Example of measurements obtained by the Polar Nephelometer and the PMS FSSP and 2D-C probes. Data obtained near the cloud top at 2300 m (MSL) with a temperature of −15°C during a 1 minute duration for the stratocumulus cloud observed on 30 January 1999. (left) Direct FSSP and 2D-C size-distributions (histogram representation) with values of the pertinent microphysical and optical parameters (*LWC*, liquid water content; *Conc*, cloud droplet concentration; *Deff*, effective diameter; *C2D*, ice particle concentration; *IWC*, ice water content; *σext*, extinction coefficient; *g*, asymmetry parameter). (right) Mean scattering phase function measured by the Polar Nephelometer (open circle symbols) and scattering phase function obtained by Mie theory (line) calculated with the average droplet size distribution measured by the FSSP over the same time period. An example of ice particle images sampled by the 2D-C probe is given in the upper right corner.

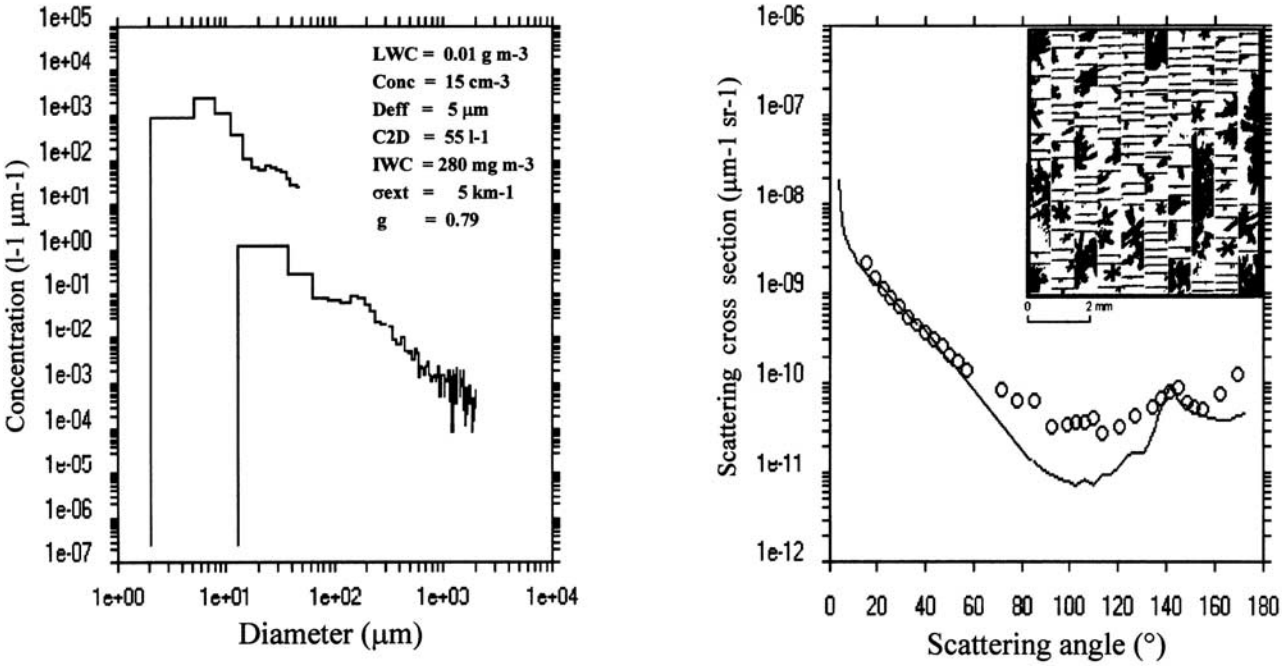

Figure 16. Same as Figure 15, but for data obtained near the cloud top at 2300 m (MSL) with a temperature of −15°C during another 1 minute duration.

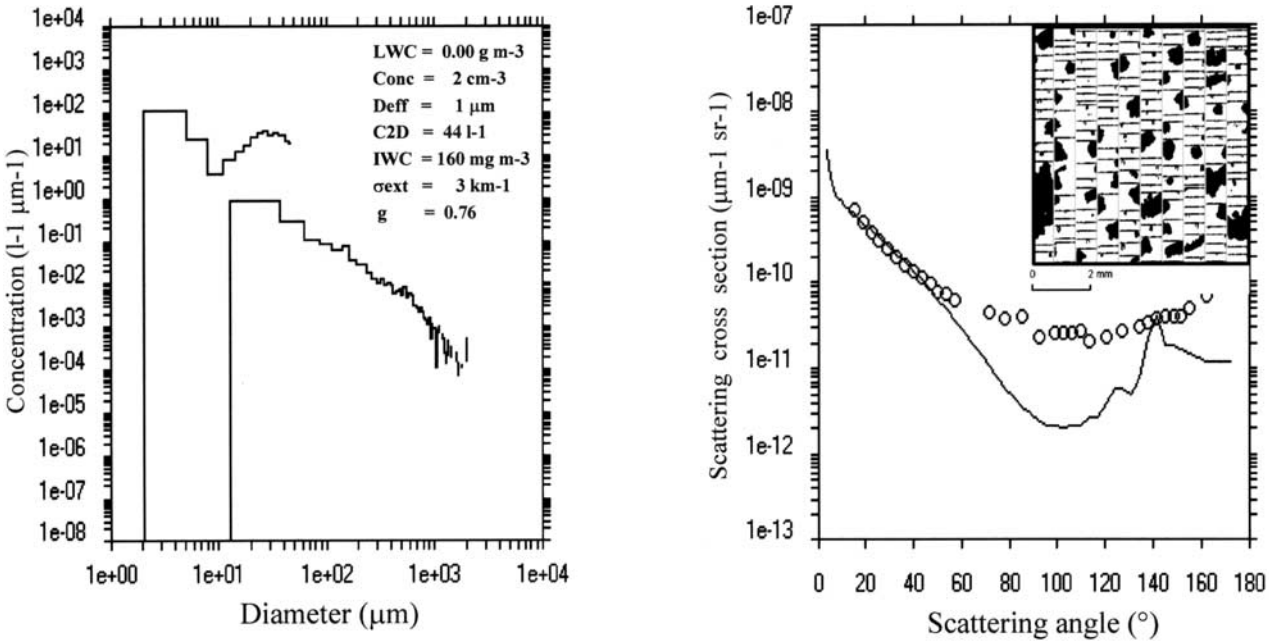

Figure 17. Same as Figure 15, but for data obtained in a precipitating region at 900 m (MSL) with a temperature of −6°C during 1 minute duration.

over the Japan Sea strongly contrast with those of the former supercooled water cloud. Due to a lower cloud top temperature (−15°C), ice crystals were found throughout the cloud level, leading subsequently the cloud to be in heavily mixed-phase condition. The direct measurement of the scattering phase functions by the Polar Nephelometer showed that ice particles strongly affected the cloud optical properties of the mixed-phase cloud, where large number of liquid water droplets with higher extinction coefficients and asymmetry factors were converted into much smaller number of larger ice crystals with smaller extinction coefficients and asymmetry factors. The mixed-phase condition explains the observed heterogeneities of the microphysical and optical properties. On the other hand, a quasi stable, liquid-droplet-prevailing cloud-top-layer was observed, where ice particles were formed and precipitated. This feature may play an important role in cloud radiative properties. Furthermore, because the scattering properties near the cloud top were mostly dominated by water droplets, the interpretation of satellite retrievals of mixed-phase clouds may suffer serious limitations in the inference of cloud compositions.

[40] The scattering phase functions measured for the first time for mixed-phase boundary layer cloud will serve as unique and valuable data set for implementation and validation of an iterative method, based on the bi-component (water and ice crystals) representation of cloud composition, for the retrieving of the microphysical properties. The measured visible and near-infrared solar absorption is discussed in detail in the companion of this paper [*Asano et al.*, 2002] with the interpretation of the results from a numerical simulation study.

[41] **Acknowledgments.** We are very grateful to Y. Mano, J. F. Fournol and the crew of B200 and C404 aircraft (Nakanihon Air Service Co., Ltd) for their helpful collaboration in the JACCS field experiment in January 1999. We also thank S. Oshchepkov and G. Febvre for their kind help in the data analysis. Thanks are extended to M. Chiba of MRI for his cooperation in the back trajectory analysis. We are very grateful to H. Isaka, Director of the LaMP, for his helpful suggestions and discussions about this project. The JACCS program is supported by the Science and Technology Agency of Japanese Government. We are grateful to anonymous reviewers for their helpful comments.

References

Asano, S., and JACCS/MRI Research Group, Japanese Cloud Climate Study (JACCS): Research plan and preliminary results, paper presented at 8th Conference on Atmospheric Radiation, Am. Meteorol. Soc., Nashville, Tenn., 23–28 Jan. 1994.

Asano, S., A. Uchiyama, Y. Mano, M. Murakami, and Y. Takayama, No evidence for solar absorption anomaly by maritime water clouds through collocated aircraft measurements, *J. Geophys. Res.*, *105*, 14,761–14,775, 2000.

Asano, S., A. Uchiyama, A. Yamazaki, J.-F. Gayet, and M. Tanizono, Two case studies of winter continental-type water and mixed-phase stratocimuli over the sea, 2, Absorption of solar radiation, *J. Geophys. Res.*, *107*, doi:10.1029/2001JD001108, in press, 2002.

Auriol, F., Mesure in situ de la fonction de phase de diffusion des particules nuageuses au moyen du Néphélomètre Polaire aéroporté: Validation et application aux nuages glacés, thèse de l'Univ. Blaise Pascal, 151 pp., Clermont-Ferrand, France, 17 Dec. 1998.

Baumgardner, D., An analysis and comparison of five water droplet measuring instruments, *J. Clim. Appl. Meteorol.*, *22*, 891–910, 1983.

Baumgardner, D., W. Strapp, and J. E. Dye, Evaluation of the Forward Scattering Spectrometer Probe, part II, Corrections for coincidence and dead-time losses, *J. Atmos. Oceanic Technol.*, *2*, 626–632, 1985.

Buriez, J. C., C. Vanbauce, F. Parol, P. Goloub, M. Herman, B. Bonnel, and Y. Fouquart, Cloud detection and derivation of cloud properties from POLDER, *Int. J. Remote Sens.*, *18*, 2785–2813, 1997.

Choularton, T. W., D. J. Griggs, B. Y. Humood, and J. Latham, Laboratory studies of riming, and its relation to splinter production, *Q. J. R. Meteorol. Soc.*, *106*, 367–374, 1980.

Crépel, O., J.-F. Gayet, J.-F. Fournol, and S. Oshchepkov, A new airborne polar nephelometer for the measurements of optical and microphysical cloud properties, part II, Preliminary tests, *Ann. Geophys.*, *15*, 460–470, 1997.

Foot, J. S., Some observations of the optical properties of clouds, I, Stratocumulus, *Q. J. R. Meteorol. Soc.*, *114*, 129–144, 1988.

Fouquart, Y., J. C. Buriez, and M. Herman, The influence of boundary layer clouds on radiation: A review, *Atmos. Res.*, *23*, 203–228, 1989.

Gayet, J.-F., P. R. Brown, and F. Albers, A comparison on in-cloud mea-

surements obtained with six PMS 2D-C probes, *J. Atmos. Oceanic Technol.*, *10*, 180–194, 1993.

Gayet, J.-F., G. Febvre, and H. Larsen, On the reliability of the PMS FSSP probe in the presence of small ice crystals, *J. Atmos. Oceanic Technol.*, *13*, 1300–1310, 1996a.

Gayet, J.-F., G. Febvre, G. Brogniez, H. Chepfer, W. Renger, and P. Wendling, Microphysical and optical properties of cirrus and contrails: Cloud field study on 13 October 1989, *J. Atmos. Sci.*, *53*, 126–138, 1996b.

Gayet, J.-F., O. Crépel, J.-F. Fournol, and S. Oshchepkov, A new airborne polar nephelometer for the measurements of optical and microphysical cloud properties, part I, Theoretical design, *Ann. Geophys.*, *15*, 451–459, 1997.

Gerber, H., Measurement of the asymmetry parameter and optical extinction coefficient of ice crystals and water droplets, final report, *NAS1-20506*, 23 pp., NASA Langley Res. Cent., Hampton, Va., 1996.

Gerber, H., B. G. Arends, and A. S. Ackerman, New microphysics sensor for aircraft use, *Atmos. Res.*, *31*, 235–252, 1994.

Gerber, H., Y. Takano, T. J. Garrett, and P. V. Hobbs, Nephelometer measurements of the asymmetry parameter, volume extinction coefficient and backscatter ratio in Artic clouds, *J. Atmos. Sci.*, *57*, 3021–3034, 2000.

Hallet, J., and S. C. Mossop, Production of secondary particles during the riming process, *Nature*, *249*, 26–28, 1974.

Harrington, J. Y., T. Reisin, W. R. Cotton, and S. M. Kreidenweis, Cloud resolving simulations of Arctic stratus, part II, Transition-season clouds, *Atmos. Res.*, *51*, 45–75, 1999.

Heymsfield, A., Microphysical structures of stratiform and cirrus clouds, in *Aerosol-Cloud-Climate Interactions*, edited by P. V. Hobbs, pp. 97–121, Academic, San Diego, Calif., 1993.

Hobbs, P. V., and A. Rangno, Ice particle concentrations in clouds, *J. Atmos. Sci.*, *42*, 2523–2549, 1995.

Hobbs, P. V., and A. Rangno, Microstructures of low and middle-level clouds over the Beaufort Sea, *Q. J. R. Meteorol. Soc.*, *124*, 2035–2071, 1998.

Larsen, H. R., J.-F. Gayet, G. Febvre, H. Chepfer, and G. Brogniez, Measurement errors in cirrus cloud microphysical properties, *Ann. Geophys.*, *16*, 266–276, 1998.

Liou, K. N., and Y. Takano, Light scattering by non-spherical particles: Remote sensing and climatic implications, *Atmos. Res.*, *31*, 271–298, 1994.

Liou, K. N., Y. Takano, and P. Yang, Light scattering and radiative transfer in ice crystal clouds: Applications to climate research, in *Light Scattering by Nonspherical Particles: Theory, Measurements and Geophysical Applications*, edited by M. I. Mishchenko, J. W. Hovenier, and L. D. Travis, pp. 417–449, Academic, San Diego, Calif., 2000.

Macke, A., P. N. Francis, G. M. McFarquhar, and S. Kinne, The role of ice particle shapes and size distributions in the single scattering properties of cirrus clouds, *J. Atmos. Sci.*, *55*, 2874–2883, 1998.

Nicholls, S., and J. Leighton, An observational study of the structure of stratiform cloud Sheets, I, Structure, *Q. J. R. Meteorol. Soc.*, *112*, 431–460, 1986.

Oshchepkov, S. L., O. V. Dubovik, and T. V. Lapyonok, A method of numerical solution of line-inverse problem with log-normal noise distribution: The estimation of aerosol size distribution, in *IRS'92: Current Problems in Atmospheric Radiation*, pp. 334–337, A. Deepak, Hampton, Va., 1993.

Raga, G. B., and P. R. Jonas, On the link between cloud-top radiative properties and sub-cloud aerosol concentrations, *Q. J. R. Meteorol. Soc.*, *119*, 1419–1425, 1993a.

Raga, G. B., and P. R. Jonas, Microphysical and radiative properties of small cumulus clouds over the sea, *Q. J. R. Meteorol. Soc.*, *119*, 1399–1417, 1993b.

Renault, S., Optimisation des méthodes de traitement et d'analyse des mesures microphysiques obtenues au moyen des sondes PMS, rapport de stage de diplome d'études approfondies, Lab. de Météorol. Phys., Univ. Blaise Pascal, Clermont-Ferrand, France, June 1998.

Riedi, J., M. Doutriaux-Boucher, P. Goloub, and P. Couvert, Global distribution of cloud top phase from POLDER/ADEOS I, *Geophys. Res. Lett.*, *27*, 1707–1710, 2000.

Sassen, K., and K. N. Liou, Scattering of polarized laser light by water droplet, mixed-phase and ice crystal clouds, part I, Angular scattering pattern, *J. Atmos. Sci.*, *36*, 838–851, 1979.

Sassen, K., G. G. Mace, Z. Wang, M. R. Poellot, S. M. Sekelsky, and R. E. McIntosh, Continental stratus clouds: A case study using coordinated remote sensing and aircraft measurements, *J. Atmos. Sci.*, *14*, 2345–2358, 1999.

Stephens, G. L., and S.-C. Tsay, On the cloud absorption anomaly, *Q. J. R. Meteorol. Soc.*, *116*, 671–704, 1990.

Takano, Y., and K. N. Liou, Solar radiative transfer in cirrus clouds, part I, Single-scattering and optical properties of hexagonal ice crystals, *J. Atmos. Sci.*, *46*, 3–18, 1989.

Takano, Y., and K. N. Liou, Radiative transfer in cirrus clouds, part III, Light scattering by irregular ice crystals, *J. Atmos. Sci.*, *52*, 818–837, 1995.

S. Asano, Center for Atmospheric and Oceanic Studies, Tohoku University, Sendai 980-8578, Japan. (s-asano@mail.cc.tohoku.ac.jp)

F. Auriol, O. Jourdan, and J.-F. Gayet, Laboratoire de Météorologie Physique, CNRS UMR 6016, Université Blaise Pascal, 24 avenue des Landais, 63177 Clermont-Ferrand Cedex, France. (gayet@opgc.univ-bpclermont.fr)

A. Sinyuk, Stepanov Institute of Physics, National Academy of Science of Belarus, 68 F. Scariny prosp., Minsk 220072, Belarus.

A. Uchiyama and A. Yamazaki, Meteorological Research Institute, Tsukuba, Ibaraki 305-0052, Japan.